JOURNAL OF PROPULSION AND POWER
Vol. 23, No. 4, July–August 2007

Kinetic Analysis of Thermite Reactions in Al–MoO_3 Nanocomposites

Mirko Schoenitz,* Swati Umbrajkar,† and Edward L. Dreizin‡
New Jersey Institute of Technology, Newark, New Jersey 07102

DOI: 10.2514/1.24853

Reactions in energetic Al–MoO_3 nanocomposites prepared by arrested reactive milling were investigated by scanning calorimetry and heated filament ignition experiments. The calorimetry data were processed to obtain kinetic parameters describing the reaction between Al and MoO_3. The reaction was treated as a combination of four subreactions, which were described by a combination of a diffusion-controlled reaction model and first-order reactions. The activation energies determined in this study allowed the comparison to reference values for the decomposition of MoO_3 and the diffusion of oxygen through an Al_2O_3 product layer. The kinetic model was extrapolated to high heating rates in the 10^3–10^6 K/s range and compared to ignition data. It was concluded that ignition of Al–MoO_3 nanocomposites prepared by arrested reactive milling is primarily controlled by oxygen diffusion in Al_2O_3.

I. Introduction

NANOMETER-SCALED metallic energetic materials have gained relevance in recent years due to their potentially very high reaction rates [1–4]. Systematic efforts have been conducted on their synthesis, for example, by mixing of nanopowder components [1], sol-gel processing [2], layer deposition [3], or arrested reactive milling [4]. To use these materials in propellants, explosives, or pyrotechnics, their reaction behavior must be known at the operating conditions of a specific application. Combustion applications are generally characterized by high heating rates in the range 10^3–10^6 K/s. Reactions at low temperatures under static conditions are relevant for storage and aging of these materials. Experimental investigations of reaction mechanisms in nanometer-scaled thermites are generally conducted by thermal analysis, and are therefore limited to low heating rates in the relatively narrow range of 0.01–1 K/s. The phenomena observed by thermal analysis frequently indicate several concurrent exothermic and endothermic processes that are difficult to separate, and therefore difficult to project to slower or faster heating regimes [5]. While separate experiments in fast heating regimes, as relevant for ignition and combustion processes result in descriptive parameters useful for applications in the range of heating rates covered, the data are difficult to reduce to obtain conclusive evidence for specific reaction mechanisms [6]. The present study uses both thermal analysis and high heating rate ignition experiments to quantify the ignition kinetics and identify the related reaction mechanism. Stoichiometric Al–MoO_3 nanocomposite powders are selected for this initial investigation. In the future, ignition kinetics for other nanocomposite reactive materials will be studied using a similar approach.

II. Experimental

Nanocomposite thermite powders with balanced $2Al + MoO_3$ composition were prepared by arrested reactive milling [7]. The synthesis of reactive nanocomposites by mechanical milling has been documented for a number of thermite systems as well as materials with highly exothermic formation of intermetallic phases [4]. The specific material for this study was prepared by milling of the component powders in 50-ml steel vials using a SPEX 8000D shaker mill. The component powders were reagent-grade materials of −325 mesh nominal size (Al, 99.8%, Atlantic Equipment Engineers; MoO_3, 99.5%, Alfa Aesar). Steel balls of 5 mm diameter were used as a milling media, and the charge ratio was 5. Milling for 60 min was carried out with 8 mL of hexane as a process control agent. The resulting nanocomposite powders were characterized by x-ray diffraction (XRD) and scanning electron microscopy [8]. Figure 1 shows a representative backscattered electron image of an Al–MoO_3 nanothermite. The sample was embedded into epoxy and cross sectioned. The phase contrast within the particles shows the formation of fully dense composites of Al and MoO_3 mixed on the scale of under 100 nm.

Reactions occurring in the nanothermites during slow heating were characterized by differential scanning calorimetry (DSC) using a Netzsch STA409PC thermal analyzer. Platinum sample pans covered with lids were used, and the furnace was flushed with argon at approximately 10 ml/min. DSC traces were recorded with heating rates varying from 1 to 5 K/min. The temperature range was limited to a maximum of 1013 K (740°C) to avoid melting and decomposition of MoO_3 above 1068 K (795°C), which could be damaging to the furnace. After the initial heating cycle, the same sample was held at 1013 K for 30 min, cooled to room temperature at 40 K/min, and then heated again at the same heating rate to obtain a baseline for the measurement. It was assumed that the bulk heat capacity of the sample did not change dramatically between the first and second heatings.

Samples were analyzed by XRD to determine the phase makeup after the heating cycle. To gain insight into the reaction process, some material was recovered after heating to intermediate temperatures, and subsequently subjected to the same phase analysis procedure. The XRD patterns were processed using the GSAS whole pattern fitting software package [9].

In addition to thermal analysis, a preliminary investigation of ignition at high heating rates in the range 10^2–10^4 K/s was conducted. A suspension of the reactive powder in hexane was coated on an electrically heated Nichrome filament (0.5 mm diam) and allowed to dry. The temperature of the filament was monitored with an infrared pyrometer. Light emission from the powder coating was detected by a photodiode. A sharp onset of the light emission was taken as evidence of ignition. The setup is illustrated in Fig. 2, and details of the experiment have been described elsewhere [10]. The

Received 28 April 2006; revision received 9 April 2007; accepted for publication 10 April 2007.

*Assistant Research Professor, Department of Mechanical Engineering.
†Doctoral Student (now graduated), Department of Mechanical Engineering.
‡Professor, Department of Chemical Engineering.

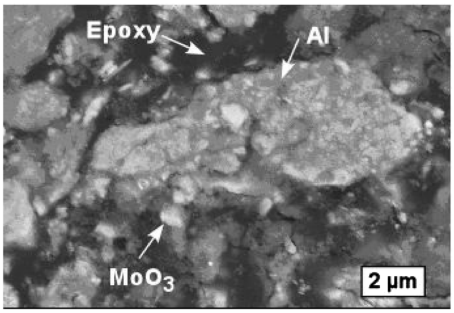

Fig. 1 Backscattered electron image of an Al–MoO_3 nanothermite prepared by arrested reactive milling. Bright areas correspond to MoO_3, medium gray areas are Al.

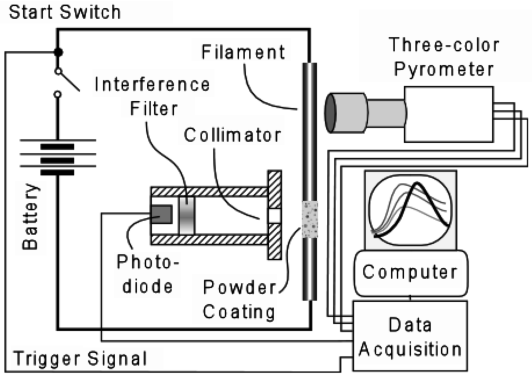

Fig. 2 Filament ignition, experimental setup (after [10]).

relation of thermal analysis and filament ignition experiments will be discussed further.

III. Results

The result of the thermal analysis is shown in Fig. 3 for several heating rates. The traces shown were baseline corrected by subtracting the DSC signal recorded for the second heating of the same sample. The thermite reaction proceeds over an extended temperature interval, between 400 and 1000 K. The DSC traces show a broad exothermic hump starting at low temperatures overlapped with at least three distinguishable exothermic peaks, as labeled in Fig. 3. Qualitatively, these measurements are generally consistent with the reported DSC traces for mixed Al and MoO_3 nanopowders [11]. Note, however, that the broad exothermic hump was not observed for mixed nanopowders. Figure 3 shows that the shape of the signal and therefore the relative significance of individual component reactions changes as a function of the heating rate. As expected, the onset of the broad exothermic hump and apparent peaks shift to higher temperatures as the heating rate increases. Minor endothermic peaks are observed below 600°C at heating rates of 2.5 and 5 K/ min. These weakly endothermic processes are not expected to play a role in the ignition phenomena of interest to this study and have not been further analyzed. XRD measurements for the samples heated to different temperatures show that as the temperature increases, the amounts of MoO_3 and Al decrease while increased amounts of MoO_2 and, at higher temperatures, Al_2MoO_6 form. Formation of amorphous or poorly crystalline Al_2O_3 polymorphs cannot be reliably identified directly from the XRD patterns, but the presence of moderate amounts of amorphous oxides would not affect the observed trends. Evolution of the phases directly identified from the XRD whole pattern processing is illustrated in Fig. 4. In general, there is reasonable correlation for the reaction progress between MoO_3 and Al determined independently from DSC and XRD measurements. However, the XRD results do not provide enough details to identify the reactions causing the exothermic peaks in the DSC traces. Additional details regarding the

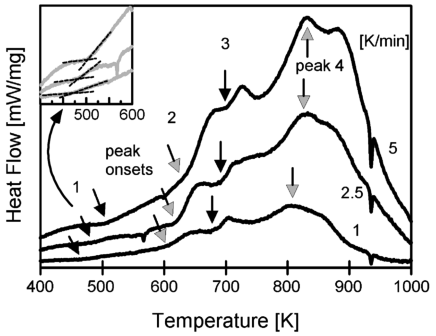

Fig. 3 Observed DSC signal for the reaction of Al–MoO_3 nanothermite at various heating rates. The endothermic peak near 930 K indicates melting of residual aluminum. The inset shows the first onsets at greater resolution.

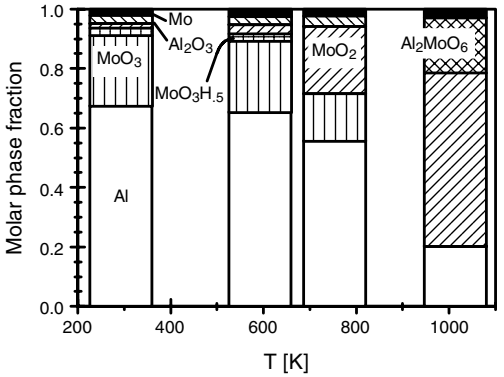

Fig. 4 Concentrations of MoO_2, MoO_3, Al, Mo, and Al_2MoO_6 determined from the whole pattern processing of the XRD measurements for the stoichiometric nanocomposite powders of $2Al + MoO_3$ heated to different temperatures.

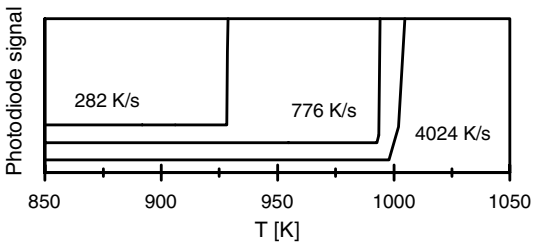

Fig. 5 Results of the ignition experiments performed at different heating rates.

comparison of the XRD and DSC measurements for the Al–MoO_3 nanocomposite thermites are reported elsewhere [8].

Example results of the ignition experiments performed at different heating rates are shown in Fig. 5. The photodiode signals are plotted versus the filament temperatures measured simultaneously. The heating rates were adjusted by varying the voltage applied to the filament and measured from the recorded pyrometer traces. The records of light emission from the igniting samples show very sharp onsets at the respective ignition temperatures. As in the thermal analysis experiments, the ignition temperature increases with increasing heating rate.

For initial evaluation, thermal analysis as well as ignition results were processed according to an isoconversion method after Kissinger [12]. Figure 6 shows the corresponding plot of $\ln(T^2/\beta)$ vs the reciprocal temperature for ignition temperature as well as for traceable DSC peaks. In this formalism, β is the heating rate in K/s and the temperatures T are derived from thermal analysis at specific reference points of exothermic peaks, and from the ignition experiments at the onset of the photodiode signal jump. The slopes of

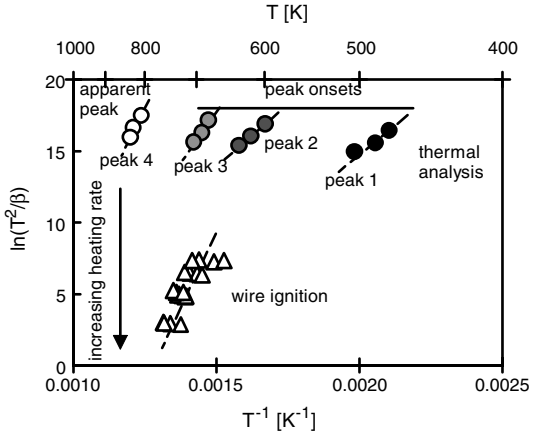

Fig. 6 Isoconversion analysis of DCS and ignition data.

these curves give an approximation of the respective activation energies of the underlying processes. Not all identified peaks were equally well resolved by thermal analysis, and therefore reference points were chosen accordingly: onsets could be identified for peaks 1, 2, and 3, while the peak maximum was used for peak 4. Assuming that each individual peak is characterized by a unique activation energy, the choice of reference point has negligible influence on the slope in Fig. 6.

Figure 6 shows that the ignition results do not line up directly with the thermal analysis. Therefore, a more detailed data processing is needed to establish the correlation between these two experiments and to identify the exothermic process (or processes) driving ignition in these materials.

IV. Data Processing

Because simple isoconversion processing did not lead to a meaningful relation between ignition and thermal analysis measurements, it was attempted to reconstruct the whole heat flow signal for the DSC measurement with the best resolution. Because activation energy and frequency factor for each individual DSC peak are relatively strongly correlated, the results of this determination were used as initial estimates only; comparison with measurements at higher heating rates allowed tuning these values.

Before more detailed data processing can be applied, the following considerations should be taken into account. From concurrent and previous work [8] it was known that the nanocomposite is relatively inhomogeneous. That is, the as-milled material contains minor contaminants aside from the major constituents. Specifically, small but noticeable amounts of $MoO_{2.5}(OH)_{0.5}$ form as a result of milling. Although its formation mechanism has not yet been unambiguously determined, it is possible that the strong mechanical activation of the milled Al causes the process control agent hexane to break down, forming poorly crystalline aluminum carbide phases while releasing hydrogen. This suggests the possibility that amorphous Al–C phases are also present in the as-milled material, although they have not been detected by either XRD or SEM investigations. Further, small amounts of MoO_3 have been reduced to form MoO_2 as well as some metallic Mo. Continued milling caused these phases to come in contact with all other phases, and as a result, a large variety of different interfaces were formed. Therefore, it was expected that the actual reactions cannot usefully be modeled with traditional reaction mechanisms that were developed for reactions in homogeneous media [13]. Such mechanisms are based on the assumption that the reaction proceeds to a certain degree of completion (that is, by depletion of the reacting components). In the present case, the reaction may actually cease to proceed as a result of growing layers of reaction products, which represent significant diffusion barriers for further reaction although the bulk composition of the sample may still have significant amounts of reactive components.

As a compromise, the observed peaks were modeled as follows: without detailed a priori information about the reaction mechanism, the system was treated as undifferentiated. The entire range of the DSC measurement at 1 K/min (see Fig. 3) was divided according to the apparent individual peaks. As the simplest assumption, the observed exothermic peaks were assumed to be independent of one another. All reactions were modeled according to the equation

$$\mathbf{\Phi}(T) = Q/\beta \cdot A e^{-\frac{E_A}{RT}} \cdot f(\alpha) \tag{1}$$

where $\mathbf{\Phi}$ is the heat evolved in a temperature interval as measured by the DSC, $\mathbf{\Phi} = \mathrm{d}Q/\mathrm{d}T$, Q is the heat of the reaction, β the heating rate $\mathrm{d}T/\mathrm{d}t$, A is the frequency factor, E_A is the activation energy, R is the universal gas constant, and T is the temperature. The reaction coordinate (nominal concentration of a reacting species) is given with α. The function $f(\alpha)$ refers to the specific kinetic law describing the reaction. The heat of reaction Q was partitioned between the four individual peaks so that

$$\sum_{i=1}^{4} Q_i = Q_{\text{total}} \tag{2}$$

Q_{total} was determined from the integral over the whole DSC trace between initial and final baselines. The requirement for a useful estimate of the reaction heat dictated the choice of the measurement at 1 K/min because measurements at other heating rates did not result in a final baseline. Integration of these measurements was therefore ambiguous.

The selection of the kinetic law defining the function $f(\alpha)$ is difficult and implies prescribing a specific reaction mechanism. In the most simplified approach, a first-order reaction $f(\alpha) = \alpha$ can be assumed. More complicated reaction kinetics could be evaluated when the first-order reaction does not describe the experiments satisfactorily. Thus, the following descriptions were selected for different exothermic peaks. The broad exothermic hump could not be described by the simple power order reaction and was modeled instead as a reaction controlled by three-dimensional diffusion as described by the Jander equation [13]

$$f_1(\alpha) = 1.5\alpha^{1/3}(\alpha^{-1/3} - 1)^{-1} \tag{3}$$

The remaining sharper peaks were successfully modeled as first-order reactions:

$$f_i(\alpha) = \alpha \quad \text{where} \quad i = 2, 3, 4 \tag{4}$$

To obtain the kinetic parameters A and E_A, the model was fit to the measurement at 1 K/min using the Netzsch Thermokinetics software package [14]. The restriction to the measurement at 1 K was necessary as the measurements at higher heating rates did not result in unambiguous final baselines, and could therefore not be used for strict data fitting. Because, however, fitting a single measurement may lead to ambiguous results [15], the activation energies and frequency factors for the three sharper peaks were estimated based on the observed shift in the measurements at 2.5 and 5 K/min. Figure 7 shows the experimental data together with the individually modeled peaks as well as the sum of the modeled peaks.

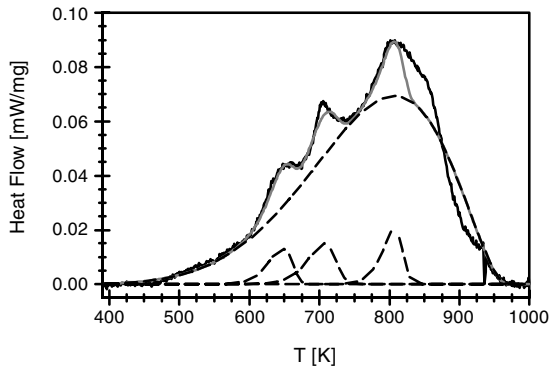

Fig. 7 Comparison of experimental data with model curves for heating rate of 1 K/min.

Table 1 Activation energies and frequency factors for individual exothermic peaks observed in the DSC traces for the stoichiometric 2Al + MO_3 nanocomposite powder

Peak no. and description	Temperature range of onset	Reaction type	E_A, kJ/mol	$\log(A\ [s^{-1}])$
1: Broad exothermic hump	470–510 K	3-D diffusion, Jander type	90	1.2
2: Exothermic peak	590–640 K	1st order	209	13.9
3: Exothermic peak	670–710 K	1st order	211	12.5
4: Exothermic peak	800–840 K (peak max.)	1st order	373	21.2

While this approach is obviously a simplification, it does allow one to evaluate the reactions at heating rates outside the range covered by thermal analysis. Therefore, once a reasonable description of the DSC traces at different heating rates is achieved, the same model can be used to describe ignition. Furthermore, because kinetics for each exothermic peak is determined it becomes possible to compare the respective activation energies to those of the known processes occurring in the specific materials system. For the Al–MoO_3 nanocomposite, related processes are the decomposition of MoO_3 and MoO_2 and diffusion of ions of O and Al through the MoO_2 and Al_2O_3 layers. Finally, it can be possible to identify one or more processes that directly control the ignition kinetics.

V. Reaction Kinetics

The kinetic parameters (frequency factors and activation energies) are shown in Table 1. To validate the calculations, the kinetic parameters were used to calculate peak positions at the highest heating rate used in thermal analysis experiments. This comparison is shown in Fig. 8. The model does not reproduce the details of the measurement; however the peak positions coincide approximately.

Projection of the model calculations to much higher heating rates is shown in Fig. 9. These calculations were compared with results of filament ignition experiments. The calculated heat flow curves were processed according to the isoconversion method after Ozawa, Flynn, and Wall (see [16] for a summary), where the temperature at a constant reaction progress $T = f(\alpha)$ is evaluated at varying heating rates β. The slope of $\ell_n(\beta)$ vs $1/T$ gives the activation energy of the rate controlling process at temperature T and heating rate β:

$$\ell_n(\beta) = \text{const} - E_A/RT \tag{5}$$

Analogous to the experimental curves, α was determined by integrating the calculated heat flow curves according to Eq. (2). Temperatures were determined for values of α in the range of 0.01–1%. Figure 10 shows the results of this calculation in relation to both experimental ignition temperatures as well as the onset of the DSC signal. The slope of the curves is similar to the ignition data points at high heating rate, while it resembles the onset of the initial reaction in the thermal analysis experiments with a low activation energy. An exact match was not obtained, but it was also not expected given the approximate nature of the presented analysis. Based on Figs. 9 and 10, it can be concluded that the ignition of the stoichiometric 2Al + MoO_3 nanocomposite powders is primarily driven by the low-activation energy process responsible for the onset of the broad exothermic hump in the DSC signal starting at low temperatures. At the same time, the processes causing sharper second and third exothermic peaks observed at higher temperatures play only a secondary role when the samples are heated rapidly. Finally, the high-activation energy process causing the fourth and strongest exothermic peak observed in the DSC traces almost does not affect ignition occurring at higher heating rates.

A more detailed analysis of the ignition is now possible in which the reaction model comprising the superposition of the four processes described in Table 1 can be used for the quantitative heat transfer analysis of the heated powder. Different experimental configurations can be readily described. For the present ignition experiments using a heated filament, it will be taken into account that the temperatures recorded are not the temperature of the reactive composite, but the temperature of the filament substrate. Recently, a numerical scheme has been developed to describe the ignition of powder coated on a heated filament [6]. Application of the reaction model developed here to this ignition simulation will be the subject of future work.

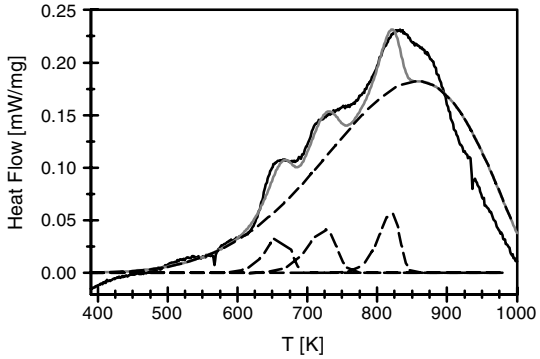

Fig. 8 Comparison of experimental data with model curves projected to heating rate of 2.5 K/min.

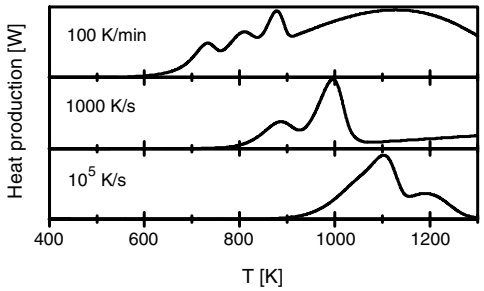

Fig. 9 Model curves projected outside the range of heating rates of thermal analysis.

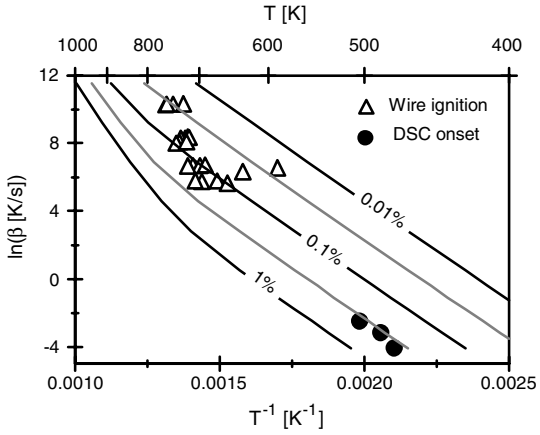

Fig. 10 Preliminary comparison of ignition experiments at high heating rates and the onset of DSC curves at low heating rates with lines of constant reaction progress calculated according to the model calculations.

VI. Discussion

The activation energies shown in Table 1 can be discussed in the context of elementary reactions in the Al–MoO_3 system. The activation energy of reduction of MoO_3 to form MoO_2 in a hydrogen atmosphere was determined as 34 kJ/mol (40 vol% H_2), or 103 kJ/mol (5 vol% H_2) [17]. The observed activation energy of the broad underlying exothermic hump is within this range, suggesting that MoO_3 reduction is the rate limiting step, at least at low temperatures. Because the comparison of MoO_3 reduction by different reducing agents may not be strictly valid, the conclusion is tentative. However, this explanation suggests that in nanothermites prepared as mixed powders the oxygen released as a result of such decomposition can readily escape. However, in dense composites as used in this study the released oxygen is contained within the condensed material and is therefore more likely to react with aluminum. This difference in the reaction process explains why the broad exothermic process observed here for the fully dense nanocomposite powders was not noticeable in the DSC traces presented in [11], for mixed nanopowders of Al and MoO_3.

The sharper and smaller peaks at higher temperatures are characterized by substantially higher activation energies, which are comparable to activation energies determined for aluminum oxidation [18]. The rates of Al oxidation depend on the surface coverage by various polymorphs of Al_2O_3 and are controlled by diffusion of ions of O and/or Al. Diffusion of oxygen through a surface layer of γ-alumina was characterized by an activation energy of 220 kJ/mol [18]. Similarly, a recent experimental study of Al oxidation by Sun et al. [11] determined an apparent activation energy of 240 ± 20 kJ/mol for Al oxidation. Activation energies as high as 418 kJ/mol were also reported for Al oxidation, without identifying the specific alumina polymorph being formed [19]. Thus, the second, third, and fourth exothermic peaks (see Table 1) could reasonably be assigned to reactions where rates are limited by diffusion through the growing alumina layer. The activation energies for the second and third peak are nearly the same, suggesting that both peaks could be caused by the diffusion through the same or similar polymorphs of Al_2O_3, most likely γ-alumina. The presence of two separate peaks could be explained by the existence of different interface morphologies where the γ-alumina (or related transition alumina) layers are being formed. The fourth peak with a high activation energy is observed at higher temperatures, at which formation of the α–Al_2O_3 polymorph is likely, and formation of the ternary phase Al_2MoO_6 is observed from XRD.

VII. Summary and Conclusions

Reactions in stoichiometric $2Al + MoO_3$ nanocomposite thermite powders have been investigated using thermal analysis and heated filament ignition experiments. A preliminary reaction model was fit to the experimental data. The reaction model is the superposition of four reaction steps assumed to be independent. The comparison of the activation energies determined for the reaction steps observed in this study with activation energies reported earlier for elementary reactions in the Al–MoO_3 system suggests that the first, low-activation energy reaction is associated with decomposition of MoO_3 while following reaction steps are controlled by the diffusion through growing layers of Al_2O_3. Preliminary comparison with ignition experiments suggests that a relatively small heat release at the onset of the exothermic reaction causes ignition at high heating rates. The proposed reaction model can be combined with a detailed heat transfer analysis for a specific experimental situation. Therefore, quantitative description of the ignition kinetics and identification of the specific reaction mechanism driving ignition for each specific experiment will become possible.

Acknowledgments

This work was supported in part by the Defense Threat Reduction Agency, Award DAAE30-01-9-0080, and the U.S. Office of Naval Research, Grant N00014-00-1-0446.

References

[1] Son, S. F, Asay, B. W., Busse, J. R., Jorgensen, B. S., Bockmon, B., and Pantoya, M. L., "Reaction Propagation Physics of Al/MoO_3 Nanocomposite Thermites," *Proceedings of the 28th International Pyrotechnics Seminar*, Defence Science & Technology Organisation, Pyrotechnics Group, 2001, pp. 833–843.

[2] Prakash, A., McCormick, A. V., and Zachariah, M. R., "Aero-Sol-Gel Synthesis of Nanoporous Iron-Oxide Particles: A Potential Oxidizer for Nanoenergetic Materials," *Chemistry of Materials*, Vol. 16, No. 8, 2004, pp. 1466–1471.

[3] Blobaum, K. J., Reiss, M. E., Plitzko Lawrence, J. M., and Weihs, T. P., "Deposition and Characterization of a Self-Propagating CuO_x/Al Thermite Reaction in a Multilayer Foil Geometry," *Journal of Applied Physics*, Vol. 94, No. 5, 2003, pp. 2915–2922.

[4] Schoenitz, M., Ward, T., and Dreizin, E. L., "Preparation of Energetic Metastable Nano-Composite Materials by Arrested Reactive Milling," *Materials Research Society Proceedings*, Vol. 800, 2003, pp. AA2.6.1–AA2.6.6.

[5] Roduit, B., Borgeat, C., Berger, B., Folly, P., Aebischer, J.-N., Andres, H., and Schaedeli, U., "Thermal Risk and Safety Margin for Energetic Materials: Assessment of Scale-Up Capabilities from Milli-(dsc) to Kilograms (Cook-Off)," *Proceedings of the 36th International Annual Conference of the ICT*, 2005, pp. 24/1–24/11.

[6] Ward, T. S., Trunov, M. A., Schoenitz, M., and Dreizin, E. L., "Experimental Methodology and Heat Transfer Model for Identification of Ignition Kinetics of Powdered Fuels," *International Journal of Heat and Mass Transfer*, Vol. 49, Nos. 25–26, 2006, pp. 4943–4954.

[7] Dreizin, E. L., and Schoenitz, M., "Nano-Composite Energetic Powders Prepared by Arrested Reactive Milling," U.S. Patent Application 20060053970, Priority: filed 12 Nov. 2004; Published by the U.S. Patent and Trademark Office on 16 March 2006, data available online at http://www.freepatentsonline.com/20060053970.html.

[8] Umbrajkar, S. M., Schoenitz, M., and Dreizin, E. L., "Control of the Structural Refinement and Composition in Al-MoO_3 Nanocomposites Prepared by Arrested Reactive Milling," *Propellants Explosives and Pyrotechnics*, Vol. 31, No. 5, 2006, pp. 382–389.

[9] Larson, A. C., and Von Dreele, R. B., "General Structure Analysis System (GSAS)," Los Alamos National Laboratory Rept. LAUR, 2000, pp. 86–748.

[10] Shoshin, Y. L., Trunov, M. A., Zhu, X., Schoenitz, M., and Dreizin, E. L., "Ignition of Aluminum-Rich Al–Ti Mechanical Alloys in Air," *Combustion and Flame*, Vol. 144, No. 4, 2006, pp. 688–697.

[11] Sun, J., Pantoya, M. L., and Simon, S. L., "Dependence of Size and Size Distribution on Reactivity of Aluminum Nanoparticles in Reactions with Oxygen and MoO_3," *Thermochimica Acta*, Vol. 444, No. 2, 2006, pp. 117–127.

[12] Kissinger, H. E., "Reaction Kinetics in Differential Thermal Analysis," *Analytical Chemistry*, Vol. 29, 1957, pp. 1702–1706.

[13] Opfermann, J., "Kinetic Analysis Using Multivariate Non-Linear Regression. I. Basic Concepts," *Journal of Thermal Analysis and Calorimetry*, Vol. 60, No. 2, 2000, pp. 641–658.

[14] Opfermann, J., NETZSCH Thermokinetics 2, Ver. 2005.04 NETZSCH Gerätebau GmbH.

[15] Maciejewski, M., "Computational Aspects of Kinetic Analysis. Part B: The ICTAC Kinetics Project—The Decomposition Kinetics of Calcium Carbonate Revisited, or Some Tips on Survival in the Kinetic Minefield," *Thermochimica Acta*, Vol. 355, Nos. 1–2, 2000, pp. 145–154.

[16] Vyazovkin, S, "Modification of the Integral Isoconversional Method to Account for Variation in the Activation Energy," *Journal of Computational Chemistry*, Vol. 22, No. 2, 2001, pp. 178–183.

[17] Ressler, T., Jentoft, R. E., Wienold, J., Günter, M. M., and Timpe, O., "In Situ XAS and XRD Studies on the Formation of Mo Suboxides During Reduction of MoO_3," *Journal of Physical Chemistry*, Vol. B104, No. 27, 2000, pp. 6360–6370.

[18] Trunov, M. A., Schoenitz, M., Zhu, X., and Dreizin, E. L., "Effect of Polymorphic Phase Transformations in Al_2O_3 Film on Oxidation Kinetics of Aluminum Powders," *Combustion and Flame*, Vol. 140, No. 4, 2005, pp. 310–318.

[19] Mitin, B. S., and Samoteikin, V. V., "Oxidation of Molten Aluminum," *Zhurnal Fizicheskoi Khimii (J. Phys. Chem.)*, Vol. 45, No. 3, 1971, p. 730 (in Russian).

S. Son
Associate Editor